ENERGY BANDS OF TlSe AND TlInSe$_2$ IN TIGHT BINDING MODEL

A THESIS SUBMITTED TO

THE GRADUATE SCHOOL OF NATURAL AND APPLIED SCIENCES

OF

MIDDLE EAST TECHNICAL UNIVERSITY

BY

ÖZLEM YILDIRIM

IN PARTIAL FULFILLMENT OF THE REQUIREMENTS

FOR

THE DEGREE OF MASTER OF SCIENCE

IN

PHYSICS

SEPTEMBER 2005

Approval of the Graduate School of Natural and Applied Sciences.

<div align="center">

_____

Prof. Dr. Canan Özgen
Director

</div>

I certify that this thesis satisfies all the requirements as a thesis for the degree of Master of Science.

<div align="center">

_____

Prof. Dr. Sinan Bilikmen
Head of Department

</div>

This is to certify that we have read this thesis and that in our opinion it is fully adequate, in scope and quality, as a thesis for the degree of Master of Science.

<div align="center">

_____

Prof. Dr. Şinasi Ellialtıoğlu
Supervisor

</div>

Examining Committee Members

Prof. Dr. Nizami Hasanli   (METU, PHYS) _____

Prof. Dr. Şinasi Ellialtıoğlu   (METU, PHYS) _____

Assoc. Prof. Dr. Oğuz Gülseren   (BILKENT, PHYS) _____

Assoc. Prof. Dr. Enver Bulur   (METU, PHYS) _____

Assist. Prof. Dr. Sadi Turgut   (METU, PHYS) _____

I hereby declare that all information in this document has been obtained and presented in accordance with academic rules and ethical conduct. I also declare that, as required by these rules and conduct, I have fully cited and referenced all material and results that are not original to this work.

Name, Last name : Özlem YILDIRIM

Signature   :

ABSTRACT

ENERGY BANDS OF TlSe AND TlInSe$_2$ IN TIGHT BINDING MODEL

Yildirim, Özlem

M. S., Department of Physics

Supervisor: Prof. Dr. Şinasi Ellialtıoğlu

September 2005, 47 pages

The electronical and structural properties of TlSe-type chain-like crystals are the main topic of this study. A computational method which is Tight Binding method is introduced and used to obtain the electronic band structure of TlSe and TlInSe$_2$. For both materials the partial and total density of states are calculated. The results are compared with the other theoretical results.

Keywords: TlSe, TlInSe, tight binding method, electronic band structure, density of states, effective mass

ÖZ

TlSe VE TlInSe$_2$'İN SIKI BAĞ MODELİNDE ENERJİ BANTLARI

Yildirim, Özlem

Yüksek Lisans, Fizik Bölümü

Tez Yöneticisi: Prof. Dr. Şinasi Ellialtıoğlu

Eylül 2005, 47 sayfa

Bu çalısmanın ana konusunu TlSe tipi zincirsi kristallerin elektronik ve yapısal özellikleri oluşturmaktadır. TlSe ve TlInSe$_2$'in elektronik bant yapıları sıkı bağ metodu kullanılarak incelendi ve bu metot ayrıntılı olarak anlatıldı. Her iki malzeme için kısmi ve toplam elektron durum yoğunlukları hesaplandı. Sonuçlar diğer kuramsal sonuçlarla karşılaştırıdı.

Anahtar Kelimeler: TlSe, TlInSe, sıkı bağ yöntemi, elektronik bant yapısı, durum yoğunluğu, etkin kütle

To my mother..

ACKNOWLEDGMENTS

TABLE OF CONTENTS

LIST OF TABLES

LIST OF FIGURES

CHAPTER I

INTRODUCTION

The understanding of the physical properties of molecular systems and bulk materials on an atomistic level is one of the fundamental tasks of physics and chemistry. The role of computational methods in this challenging task is steadily increasing as a result of both the rapid progress in computer performance and the algorithmic advances in the field. Many computational methods are nowadays used in materials science for electronic structure calculations. These methods span from very accurate quantum chemistry techniques applied to small molecules up to empirical schemes which make it possible to simulate systems composed of about million atoms. The empirical tight-binding method of modeling electronic structures of materials is not to be compared with the very accurate, expensive, and reliable *ab initio* methods, however, it is preferred or can be the only way out when the size of the problem is much larger and when speed is important.

Because of the important role of semiconductors in technology, they are the most widely investigated materials and still attract attention of many scientists. The semiconductors are distinguished from the other materials, namely, insulators and conductors, due to the special character of their electronic structure. One can tell the difference between conductors, insulators and semiconductors by visualizing the available energies for electrons in the materials. Unlike the free atoms having discrete energies, the available energy states form bands. The highest energy band group occupied by electrons in their ground state is called the valence band. The lowest energy band group occupied by excited electrons and empty otherwise (in the ground state) is called the conduction band. The energy spacing between the valence band and the conduction band is called the (forbidden) band gap. An important parameter in the band theory is the Fermi level, the top of the available electron energy levels at absolute zero. The position of the Fermi level in relation to the conduction band is a crucial factor in determining the electronic properties. In insulators the magnitude of the band gap is quite large (typically few to 10 eV) that conductivity is negligible, while the gap of semiconductors is smaller (of the order of an eV), and some conductivity is observed at finite temperatures. The lowest excitation consists of promoting an electron from the valence band to the conduction band. This results in an electron being near the bottom of the conduction band and a hole near the top of the valence band. It is important to know the values such as band gap, concentration of

electrons in the conduction bands, and that of the holes in the valence bands in order to characterize the electronic behavior of a semiconductor material.

Semiconductors are available as either elemental materials or as compounds. The most common elemental semiconductors are silicon and germanium. Silicon and germanium have diamond structure and there is a whole electronic technology set up based on silicon. Compound semiconductors that are widely studied are of III-V groups in zinc-blende structure, and include GaAs, InSb, InAs, GaP, etc. With the advent of epitaxial growth, GaAs is used in semiconductor laser applications. The advantage of compound semiconductor is that the energy gaps span a wide range, so that materials are available with properties that meet specific requirements of the device engineer. The combination of silicon technology and lasing talent of GaAs is a promising marriage for optoelectronic devices and nanotechnology.

Another type of compounds that are considered as the topic of this study are the III-VI compounds, which are of chain-like or of layered structures. These materials attracted interest of many researchers because of their possible technological applications such as switching and memory devices, oscillators, thermistors, etc. Their low dimensionality makes these materials important in fields like photoconductivity, optoacoustics and optoelectronics. Among them TlSe is a generic material of chain-like structure and will be investigated in this work. We concentrate on their electronic properties and using a simple tight binding model we determine their electronic band structure and corresponding

density of states.

In the following chapter the tight-binding theory is discussed, and how the tight-binding matrix elements can be obtained is introduced in detail, and the effective mass values of electrons and holes are estimated and compared with values in the existing literature.

After the theory, in the third chapter, the structural properties of chain-like compounds with a special interest on TlSe and $TlInSe_2$ are introduced. The crystal structure and the previous studies concerning these materials are mentioned.

In the fourth chapter, the results of the tight-binding calculation fitted to band structures obtained by other means are introduced. To achieve these results, firstly, the hopping parameters are found and presented in this chapter. For a better understanding of chemical bonding and the nature of the relevant atomic interactions, we have performed the density of states calculation and compared them as well. Effective masses are obtained by fitting parabolas E-bands, that are also presented in this chapter.

CHAPTER II

THEORY

The Schrödinger equation is solved exactly analytically only for a few examples like particle in a box, square barrier and wells, simple harmonic oscillator potential and the hydrogen atom. When a molecule or an atom with several electrons are in question, the exact analytical solutions are close to hopeless. In the case of solids, the periodicity of the crystal is a big advantage to carry out the calculations. With the high performance of the present day computer, the Schrödinger equation can be solved numerically using certain approximations. The *ab initio* method yields the most accurate reliable results. This method starts with the Born-Oppenheimer approximation which is based on the idea that the motion of the nuclei in a molecule or a solid is much slower than that of the electrons, due to much larger masses of the nuclei compared to electrons. There are two main approaches for the many body the calculations in the *ab initio* method. One of them is the Hartree-Fock method.

This method expresses the total wavefunction of the system as a product of one-electron orbitals which takes into account the antisymmetric nature of the total wavefunction. The other approach is the Density Functional Theory which is to replace the many-body electronic wavefunction with a functional of the electronic density. The wavefunction in the Schrödinger equation can be formed by using the Bloch sums, namely the sum of the localized atomic orbitals that are weighted with a phase which depends on the crystal momentum and periodicity of the lattice in a crystal. The atomic orbitals used for Bloch sums can be either Slater-type orbitals (STOs), Gaussian-type orbitals (GTOs), or various other numerical functions which have to form a complete orthogonal set. When plane waves are used as basis functions, the method is called the plane wave (PW) method which is used more successfully for metals. Further, one can use a set of orthogonalized plane waves (OPW) in which case the wave functions of the valence states are all orthogonal to the core states. The secular equation formed by OPWs can give only valence and conduction energies and the corresponding wave functions. To determine the core orbitals the muffin-tin potential can be adopted. In the "muffin-tin approximation", the potential seen by an electron is decomposed into two regions such as muffin-tin and muffin-pan. One is a spherically symmetric part around each atom and is called the muffin-tin. The muffin-pan is the potential in the outer region which is flat and constant. The wavefunctions in the muffin-tin are called muffin-tin orbitals. When the plane waves of the outer region are

6

matched with the muffin-tin orbitals, the method is called augmented plane wave method (APW).

A different approach used very commonly is the pseudopotential method. The pseudopotential method can be used in an ab-initio method or in an empirical fit. The main point in this approach is only the valence electrons are considered, and their interaction with the ionic cores is replaced by a pseudopotential, $v(\vec{r})$. This means in fact that the solutions of the Schrödinger equation are pseudo-wavefunctions and the charge density, $n(\vec{r})$, is the pseudo-density of the valence electrons.

In the next section, the tight binding Hamiltonian is introduced and the necessary approximations needed to solve the secular equation are discussed.

II.1   Tight-Binding Method

The tight-binding formalism is an extension of Bloch's original Linear Combination of Atomic Orbitals (LCAO) method [1], it was parametrized by Slater and Koster [2] in 1954 for certain simple lattice types including the diamond structure. After that the tight-binding method has been used very widely in many applications.

The Hamiltonian for the electron in the solid is

$$H(\vec{r}) = \frac{p^2}{2m} + V(\vec{r}), \tag{II.1}$$

where $V(\vec{r})$ is the effective one-electron potential with the lattice periodicity $V(\vec{r} + \vec{R}_j) = V(\vec{r})$.

In the tight binding or LCAO approximation, the wavefunction for the solid is constructed as a Linear Combination of Atomic Orbits. The Bloch function is

$$\psi_{\vec{k}}(\vec{r}) = \sum_\alpha C_\alpha \sum_{\vec{R}_i} \phi_\alpha(\vec{r} - \vec{R}_i)\, e^{i\vec{k}\cdot\vec{R}_i} \tag{II.2}$$

where α denotes the symmetry type of the atomic function, s, p, d, etc., and C_α are constants to be determined, $\vec{k}$ is a vector in the Brillouin zone. Since the ϕ's are atomic orbitals then the $\psi_{\vec{k}}$'s are not orthogonal functions because the constituent atomic orbitals centered at different positions $\vec{R}_i$ need not be orthogonal :

$$\int d^3r\, \phi_\alpha^*(\vec{r} - \vec{R}_i)\phi_\beta(\vec{r} - \vec{R}_j) \equiv S_{\alpha\beta}^{ij}. \tag{II.3}$$

$S_{\alpha\beta}^{ij}$ are the measures of the non-orthogonality and are called the "overlap" integrals, and the matrix $\hat{S}$, the overlap matrix.

It is convenient to work with orthogonal functions. So, one can define a set of new atomic-like basis states called Löwdin orbitals [3] by :

$$\phi_\gamma'^\dagger(\vec{r} - \vec{R}_m) \equiv \sum_{\beta j} \left(S^{-1/2}\right)_{\gamma\beta}^{mj} \phi_\beta^*(\vec{r} - \vec{R}_j) \tag{II.4}$$

and

$$\phi_{\gamma'}'(\vec{r} - \vec{R}_n) \equiv \sum_{\beta'j'} \left(S^{-1/2}\right)_{\beta'\gamma'}^{j'n} \phi_{\beta'}(\vec{r} - \vec{R}_{j'}) \tag{II.5}$$

Then, it can be shown that

$$\int \phi_\gamma'^\dagger(\vec{r} - \vec{R}_m)\, \phi_{\gamma'}'(\vec{r} - \vec{R}_n)\, d^3r = \delta_{mn}\delta_{\gamma\gamma'} \tag{II.6}$$

Now, these new functions are orthogonal. Hence, one assumes Löwdin orbitals as the basis functions, and expansion of the wave function can be named

as Linear Combinations of Löwdin Orbitals (LCLO). However, an important feature proved by Löwdin is that the symmetry of $\phi'_\gamma(\vec{r} - \vec{R}_i)$ is the same as that of $\phi_\alpha(\vec{r} - \vec{R}_i)$, the atomic orbital, meaning, group theoretically that both have identical transformation properties under the group of the Hamiltonian. Thus, for conceptual purposes we may think of these states as atomic functions.

In terms of Löwdin orbitals one has :

$$\int \psi_{\vec{k}}^{\dagger}(\vec{r})\psi_{\vec{k}'}(\vec{r})d^3r = N\delta_{kk'}\sum_\alpha |C_\alpha|^2 \tag{II.7}$$

Then, the normalization factor is $\frac{1}{\sqrt{N}}$ with the condition that $\sum_\alpha |c_\alpha|^2 = 1$ and the functions are orthogonal in k-space (i.e., $\delta_{kk'}$ factor). Thus,

$$\psi_{\vec{k}}(\vec{r}) = \frac{1}{\sqrt{N}} \sum_\alpha C_\alpha^{(\vec{k})} \sum_{\vec{R}_i} \phi_\alpha(\vec{r} - \vec{R}_i)e^{i\vec{k}\cdot\vec{R}_i} \tag{II.8}$$

is now an expansion in terms of a complete orthonormal set of functions.

To generate the secular equation we start with Schrödinger's equation

$$H(\vec{r})\psi_{\vec{k}}(\vec{r}) = E_{\vec{k}}\psi_{\vec{k}}(\vec{r}) \tag{II.9}$$

which can be put in the form

$$\sum_\alpha \sum_{\vec{R}_i} \left\{ H_{\alpha\beta}^{mi}e^{i\vec{k}\cdot(\vec{R}_i - \vec{R}_m)} - E_{\vec{k}}\delta_{\alpha\beta}\delta_{mi} \right\} C_\alpha = 0 \tag{II.10}$$

This is recognized as the usual matrix eigenvalue equation (leading to the secular equation):

$$\left(\hat{H} - \hat{E} \right) \vec{C} = 0 \tag{II.11}$$

with the Hamiltonian matrix elements (hopping integrals) defined as

$$H_{\alpha\beta}^{mi} \equiv \int \phi_\beta^*(\vec{r} - \vec{R}_m) \, H(\vec{r}) \, \phi_\alpha(\vec{r} - \vec{R}_i) \, d^3r \tag{II.12}$$

9

II.2 Near Neighbors Approximation

The largest matrix elements of $H_{\beta\alpha}^{mi}$ are the diagonal, $H_{\alpha\alpha}^{ii}$, and the nearest neighbor, $H_{\alpha\beta}^{i,i+\Delta}$, terms where $(i+\Delta)$ implies $\vec{R}_i + \vec{\Delta}$ with $\vec{\Delta}$ being a nearest neighbor vector. With this approximation (II.10) reduces to

$$\sum_\alpha \left\{ H_{\beta\alpha}^0 + \left[\sum_{\vec{\Delta}} H_{\alpha\beta}^{\vec{\Delta}} e^{i\vec{k}\cdot\vec{\Delta}} \right] - E_{\vec{k}} \delta_{\alpha\beta} \right\} C_\alpha = 0 \qquad \text{(II.13)}$$

This is a matrix equation whose dimensionality is determined by the number of different symmetry basis functions α employed.

If the second nearest neighbor interactions are also considered then the matrix equation will have the form

$$\sum_\alpha \left\{ H_{\beta\alpha}^0 + \left[\sum_{\vec{\Delta}_1} H_{\alpha\beta}^{\vec{\Delta}_1} e^{i\vec{k}\cdot\vec{\Delta}_1} \right] + \left[\sum_{\vec{\Delta}_2} H_{\alpha\beta}^{\vec{\Delta}_2} e^{i\vec{k}\cdot\vec{\Delta}_2} \right] - E_{\vec{k}} \delta_{\alpha\beta} \right\} C_\alpha = 0. \qquad \text{(II.14)}$$

where $\vec{\Delta}_1$ is the nearest-neighbor vector and $\vec{\Delta}_2$ is the second nearest neighbor vector.

Hamiltonian matrix elements, also called hopping integrals, may be difficult to calculate analytically. But they can be assigned to certain parameters which are to be determined by fitting to other model calculations or existing experimental information. The naming convention for on-site and hopping terms adopted here is as follows :

$$H_{\alpha\alpha}^0 \equiv \int \phi_\alpha^*(\vec{r}) \, H(\vec{r}) \, \phi_\alpha(\vec{r}) \, d^3r \equiv E_\alpha, \quad \alpha = s, p \qquad \text{(II.15)}$$

$$H_{ss}^{\Delta^n} \equiv \int \phi_s^*(\vec{r}) \, H(\vec{r}) \, \phi_s(\vec{r} - \Delta_z^n) \, d^3r \equiv (ss\sigma)_n \qquad \text{(II.16)}$$

$$H_{sp}^{\Delta^n} \equiv \int \phi_s^*(\vec{r}) \, H(\vec{r}) \, \phi_{p_z}(\vec{r} - \Delta_z^n) \, d^3r \equiv (sp\sigma)_n \qquad \text{(II.17)}$$

$$H_{zz}^{\Delta^n} \equiv \int \phi_{p_z}^*(\vec{r})\, H(\vec{r})\, \phi_{p_z}(\vec{r} - \Delta_z^n)\, d^3r \equiv (pp\sigma)_n \qquad \text{(II.18)}$$

$$H_{yy}^{\Delta^n} \equiv \int \phi_{p_y}^*(\vec{r})\, H(\vec{r})\, \phi_{p_y}(\vec{r} - \Delta_z^n)\, d^3r \equiv (pp\pi)_n \qquad \text{(II.19)}$$

For the ss-, sp-, pp-bondings, there are only four nonzero hopping integrals as shown in Figure II.1.
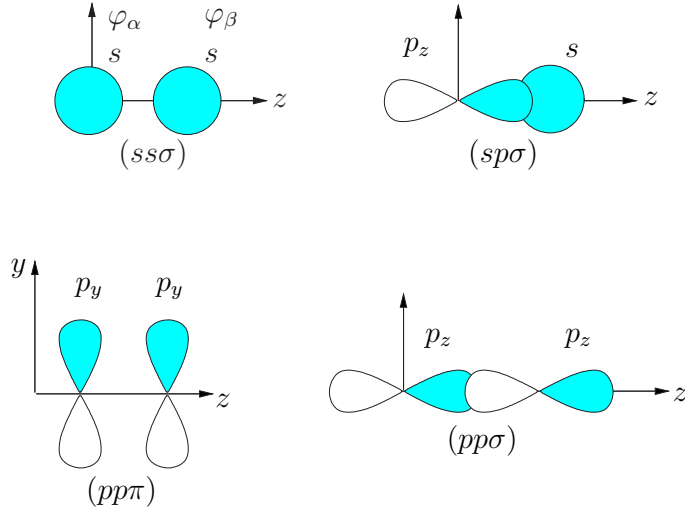
Figure II.1: Orbital interaction integrals in the two-center approximation.

II.3 Slater-Koster Model for Silicon

The on-site terms arise from the self-interaction of each orbital of the same atom i.e. when $i = j$ and $\alpha = \beta$. They contribute to the diagonal elements of the Hamiltonian matrix and can be shown $\langle s_i|H|s_i \rangle = E_s$ and $\langle p_i|H|p_i \rangle = E_p$. When i is not equal to j, interactions between orbitals on different atoms can be found for a general geometry (rather than only the special cases like in Fig.

II.1) using the equations below:

$$E_{ss}(\vec{d}) = s_1 s_2 \sigma(d)$$

$$E_{sp}(\vec{d}) = s_1 p_2 \sigma(d) \hat{d} \cdot \vec{t}_{p_2} \qquad \text{(II.20)}$$

$$E_{pp}(\vec{d}) = p_1 p_2 \sigma(d)(\hat{d} \cdot \vec{t}_{p_1})(\hat{d} \cdot \vec{t}_{p_2}) + p_1 p_2 \pi(d)(\hat{d} \times \vec{t}_{p_1}) \cdot (\hat{d} \times \vec{t}_{p_2})$$

where $\vec{d}$ is the vector from one orbital to the other, $\hat{d} = \vec{d}/|\vec{d}|$ and $\vec{t}$ is the direction of the p orbital. The p orbital has three components as p_x, p_y, and p_z, so they can be denoted as x, y, and z. With the help of equation (II.20), part of the table, including only $s - p$ orbital interactions, in the Slater and Koster paper [2] can be obtained as shown below :

$$E_{s,s} = (ss\sigma)$$

$$E_{s,x} = l(sp\sigma)$$

$$E_{x,x} = l^2(pp\sigma) + (1 - l^2)(pp\pi) \qquad \text{(II.21)}$$

$$E_{x,y} = lm(pp\sigma) - lm(pp\pi)$$

$$E_{x,z} = ln(pp\sigma) - ln(pp\pi) \ .$$

These equations are for the simple cubic unit cell, where l, m, and n are the projections along the $\vec{R}_j - \vec{R}_i$ vector with respect to x, y, and z directions, and are called directional cosines. The most popular materials as semiconductors are Si and Ge which have the diamond structure. They have been investigated in detail over the years and their electronic structure are well-known and the tight binding method gives a good description of their electronic behavior. For this reason, as a result of equation (II.20), the energy integrals are obtained

for the diamond and given in the equation (II.22) :

$$E_{ss}(\tfrac{1}{2}\tfrac{1}{2}\tfrac{1}{2}) = (ss\sigma)_1 \qquad\qquad E_{ss}(110) = (ss\sigma)_2$$

$$E_{xx}(\tfrac{1}{2}\tfrac{1}{2}\tfrac{1}{2}) = \tfrac{1}{3}(pp\sigma)_1 + \tfrac{2}{3}(pp\pi)_1 \quad E_{xx}(011) = (pp\pi)_2$$

$$E_{xy}(\tfrac{1}{2}\tfrac{1}{2}\tfrac{1}{2}) = \tfrac{1}{3}(pp\sigma)_1 - \tfrac{1}{3}(pp\pi)_1 \quad E_{xy}(110) = \tfrac{1}{2}(pp\sigma)_2 - \tfrac{1}{2}(pp\pi)_2$$

$$E_{sx}(\tfrac{1}{2}\tfrac{1}{2}\tfrac{1}{2}) = \tfrac{1}{\sqrt{3}}(sp\sigma)_1 \qquad E_{xx}(110) = \tfrac{1}{2}(pp\sigma)_2 + \tfrac{1}{2}(pp\pi)_2$$

$$E_{sx}(110) = \sqrt{2}(sp\sigma)_2$$

$$E_{sx}(011) = E_{xy}(011) = 0$$

(II.22)

Above the nearest neighbor interaction parameters are listed in the first column in terms of two-center integrals and that of the second nearest neighbor interactions in the second column.

Phase of the Matrix Elements:

According to positions of atoms in the unit cell, the exponential part will consist of cosine and sine terms. In a diamond the four first nearest neighbors of the given atom at (0,0,0) are located at the positions: $(\tfrac{1}{2}\tfrac{1}{2}\tfrac{1}{2})$, $(\tfrac{1}{2} - \tfrac{1}{2} - \tfrac{1}{2})$, $(-\tfrac{1}{2}\tfrac{1}{2} - \tfrac{1}{2})$, $(-\tfrac{1}{2} - \tfrac{1}{2}\tfrac{1}{2})$ in units of $\tfrac{a}{2}$. Therefore, the k-dependent parts of the matrix equation of the diamond for the first nearest neighbors are as follows:

$$g_0(\vec{k}) = + \cos\tfrac{k_x a}{4} \cos\tfrac{k_y a}{4} \cos\tfrac{k_z a}{4} - i\ \sin\tfrac{k_x a}{4} \sin\tfrac{k_y a}{4} \sin\tfrac{k_z a}{4}$$

$$g_1(\vec{k}) = - \cos\tfrac{k_x a}{4} \sin\tfrac{k_y a}{4} \sin\tfrac{k_z a}{4} + i\ \sin\tfrac{k_x a}{4} \cos\tfrac{k_y a}{4} \cos\tfrac{k_z a}{4}$$

$$g_2(\vec{k}) = - \sin\tfrac{k_x a}{4} \cos\tfrac{k_y a}{4} \sin\tfrac{k_z a}{4} + i\ \cos\tfrac{k_x a}{4} \sin\tfrac{k_y a}{4} \cos\tfrac{k_z a}{4}$$

$$g_3(\vec{k}) = - \sin\tfrac{k_x a}{4} \sin\tfrac{k_y a}{4} \cos\tfrac{k_z a}{4} + i\ \cos\tfrac{k_x a}{4} \cos\tfrac{k_y a}{4} \sin\tfrac{k_z a}{4}$$

(II.23)

Now, all the components of the Hamiltonian matrix of the diamond can be

written as:

$$
\begin{pmatrix}
E_{s_1} & 0 & 0 & 0 & V_{ss}\,g_0 & V_{sx}\,g_1 & V_{sx}\,g_2 & V_{sx}\,g_3 \\[2mm]
0 & E_{p_1} & 0 & 0 & -V_{sx}\,g_1 & V_{xx}\,g_0 & V_{xy}\,g_3 & V_{xy}\,g_1 \\[2mm]
0 & 0 & E_{p_1} & 0 & -V_{sx}\,g_2 & V_{xy}\,g_3 & V_{xx}\,g_0 & V_{xy}\,g_1 \\[2mm]
0 & 0 & 0 & E_{p_1} & -V_{sx}\,g_3 & V_{xy}\,g_1 & V_{xy}\,g_2 & V_{xx}\,g_0 \\[2mm]
V_{ss}\,g_0^* & -V_{sx}\,g_1^* & -V_{sx}\,g_2^* & -V_{sx}\,g_3^* & E_{s_2} & 0 & 0 & 0 \\[2mm]
V_{sx}\,g_1^* & V_{xx}\,g_0^* & V_{xy}\,g_3^* & V_{xy}\,g_1^* & 0 & E_{p_2} & 0 & 0 \\[2mm]
V_{sx}\,g_2^* & V_{xy}\,g_3^* & V_{xx}\,g_0^* & V_{xy}\,g_2^* & 0 & 0 & E_{p_2} & 0 \\[2mm]
V_{sx}\,g_3^* & V_{xy}\,g_1^* & V_{xy}\,g_1^* & V_{xy}\,g_1^* & 0 & 0 & 0 & E_{p_2}
\end{pmatrix}
\tag{II.24}
$$

where $E_s, E_p, V_{ss}, V_{xx}, V_{xy}$, and V_{sx} are defined below:

$$
\begin{aligned}
E_s &= E_{s,s}(000), & E_p &= E_{x,x}(000), \\[2mm]
V_{ss} &= 4E_{ss}(\tfrac{1}{2}\tfrac{1}{2}\tfrac{1}{2}), & V_{xx} &= 4E_{xx}(\tfrac{1}{2}\tfrac{1}{2}\tfrac{1}{2}), \\[2mm]
V_{xy} &= 4E_{xy}(\tfrac{1}{2}\tfrac{1}{2}\tfrac{1}{2}), & V_{sx} &= 4E_{sx}(\tfrac{1}{2}\tfrac{1}{2}\tfrac{1}{2}),
\end{aligned}
\tag{II.25}
$$

When we consider the second nearest neighbor interactions, the additional terms enter to the diagonal minors (4×4) of the full matrix (8×8). So the first diagonal minor becomes:

$$
M_{11} =
\begin{pmatrix}
E_{s_1} + V_{ss_2}\,g_4 & V'_{sy_2}\,g_7 + V_{sx_2}\,g_8 & \cdots & \cdots \\[2mm]
V'_{sy_2}\,g_7 + V_{sx_2}\,g_8 & E_{p_1} + V_{xx_2}\,g_5 + V'_{xx_2}\,g_6 & \cdots & \cdots \\[2mm]
\vdots & \vdots & \ddots & \\[2mm]
\vdots & \vdots & & \ddots
\end{pmatrix}
\tag{II.26}
$$

The second diagonal matrix becomes very similar to the first one, but for

some of the matrix elements the sign will be opposite :

$$
M_{22} = \begin{pmatrix}
E_{s_2} + V_{ss_2}\, g_4 & -V'_{sy_2}\, g_7 + V_{sx_2}\, g_8 & \cdots & \cdots \\
-V'_{sy_2}\, g_7 + V_{sx_2}\, g_8 & E_{p_2} + V_{xx_2}\, g_5 + V'_{xx_2}\, g_6 & \cdots & \cdots \\
\vdots & \vdots & \ddots & \\
\vdots & \vdots & & \ddots
\end{pmatrix}
$$

(II.27)

where $V_{ss_2}, V_{xx_2}, V'_{xx_2}, V_{sx_2}, V'_{sy_2}$, etc., and g_4, g_5, g_6, g_7, g_8, etc., are defined below:

$$V_{ss_2} = 4E_{ss}(110),$$

$$V_{xx_2} = 4E_{xx}(110), \quad V'_{xx_2} = 4E_{xx}(011)$$

(II.28)

$$V_{sx_2} = 4iE_{sx}(110), \quad V'_{sy_2} = -4E_{sy}(011)$$

and

$$g_4(\vec{k}) = \cos\frac{k_x a}{2}\cos\frac{k_y a}{2} + \cos\frac{k_y a}{2}\cos\frac{k_z}{2} + \cos\frac{k_x a}{2}\cos\frac{k_z a}{2}$$

$$g_5(\vec{k}) = \cos\frac{k_x a}{2}\cos\frac{k_y a}{2} + \cos\frac{k_x a}{2}\cos\frac{k_z a}{2}$$

$$g_6(\vec{k}) = \cos\frac{k_y a}{2}\cos\frac{k_z a}{2}$$

(II.29)

$$g_7(\vec{k}) = -\sin\frac{k_x a}{2}\sin\frac{k_y a}{2}$$

$$g_8(\vec{k}) = i(\sin\frac{k_x a}{2}\cos\frac{k_y}{2} + \sin\frac{k_x a}{2}\cos\frac{k_z a}{2})$$

The off-diagonal minors M_{12} and M_{21} will not be affected by the inclusion of the second nearest neighbor interactions. Finally the matrix will have the following form:

$$
\begin{pmatrix}
M_{11} & M_{12} \\
M_{21} & M_{22}
\end{pmatrix}.
$$

(II.30)

Solving for the eigenvalues of the above matrix, the energy band diagram of Si in terms of $\vec{k}$ is given in Figure II.2. To obtain the bands we have used

15
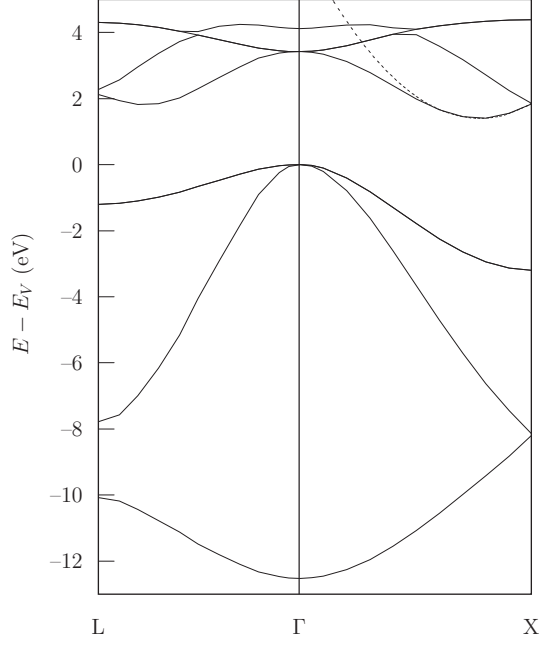
Figure II.2: Tight-binding energy band structure of Si with Pandey's parameters [4]

the two center integral parameters given in the Ref. [4]. The parameters are listed in the Table II.1.

Comparison of the results with the experimental findings indicates that the great quantitative agreement ($\approx 2\%$) for the valence bands is achieved using tight binding method [4].

Table II.1: The first and second nearest neighbor two-center integral parameters (in eV) for Si by Pandey [4].

ETB Parameters	Values for Si (in eV)
$E_p - E_s$	4.39
$(ss\sigma)_1$	–2.08
$(sp\sigma)_1$	–2.12
$(pp\sigma)_1$	–2.32
$(pp\pi)_1$	–0.52
$(pp\sigma)_2$	–0.58
$(pp\pi)_2$	–0.10

One can increase the accuracy ignoring some of the approximations used in the method. The approximations reduce the transferability. Transferability is one of the disadvantages of tight binding because, for example, a parametrization suitable for Si in the diamond structure, may not be adequate for simulating liquid Si. Starting from the first approximation, instead of orthogonal Löwdin orbitals, one can use a non-orthogonal basis set. This was first done by Mattheiss and Patel [5]. The effects of non-orthogonality of the basis have been investigated by Mirabella et al. [6] for one dimensional atomic chains in 1994, and by McKinnon and Choy [7] for two and three dimensional lattices in 1995. Since the non-orthogonal tight binding method is more realistic, many calculations have been performed to investigate and better describe the electronic properties of materials using the non-orthogonal type set.

Including the further neighbor interactions beyond first and the second can increase the accuracy. There are calculations in the literature which include the third nearest neighbor interactions as well [5].

In addition to the s and p orbitals, s^* and also d orbitals are included in various calculations. When the importance of the empty d orbitals become unavoidable, e.g. in the case of germanium conduction bands, Vogl, Hjalmarson, and Dow [8] added an s^* orbital to the sp^3 basis set to mimic the influence of the empty d states above the conduction bands. Later on Chang and Aspnes [9] made the calculations using six orbitals. They included the d^2 orbitals instead of utilizing the s^* orbital to correct the lowest conduction bands, and

achieving the same results obtained by sp^3s^* case. Jancu, Scholz, Beltram, and Bassani [10] increased the number of the basis set to ten atomic orbitals, namely $sp^3d^5s^*$. With this approach they reproduced the main features of the valence band and that of the two lowest conduction bands more successfully.

The last modification can be done by adopting the three-center integrals. Calculations that use the three-center matrix elements can achieve better fits than those that use just the two-center integrals in expressing the matrix elements. This is because there are more fitting parameters available, and moreover, some physically important contributions to the matrix elements might also be neglected in the two-center integral approximation. As a good example for the inclusion of three-center integrals, Papaconstantopoulos has found the best fits using the three center formulation to the face-centered-cubic and body-centered-cubic solids [11].

With the tight binding method discussed above, we have obtained the energy band diagram of the system. Using energy values found in terms of $\vec{k}$, total density of states, partial density of states and effective mass can be calculated. In the following two sections, the density of states and effective mass formulations will be introduced.

II.4 Density of States

The density of states (DOS) results can be directly used in finding other electrical properties of materials such as the electric heat capacity and the optical

absorbtion. The photoemission spectroscopy reflects the peak positions and other structures in density of states.

DOS can be calculated by counting the number of states at each infinitesimal energy range between E and $E + dE$. It is customary to calculate the number of states per unit energy per unit volume:

$$\rho(E) \propto \sum_{\vec{k}} \{\theta(E + \Delta E - E(\vec{k})) - \theta(E - E(\vec{k}))\} \qquad \text{(II.31)}$$

where the first θ-function counts the number of states with energies less than $E + dE$, and the second θ-function counts the number of states with energies less than E. The differences in the limit $\Delta E \rightarrow dE$ becomes a δ-function and $\rho(E)dE$ equals the number of states with energies between E and $E + dE$ per unit cell. Most generally, the density of states can be written as below:

$$\rho(E) = \frac{2\Omega_{cell}}{(2\pi)^3} \int_{BZ} \delta[E_{ij}(\vec{k}) - E]d^3k \qquad \text{(II.32)}$$

which can be put into a surface integral given as follows:

$$\rho(E) = \frac{2\Omega_{cell}}{(2\pi)^3} \int_{S} \frac{dS}{|\vec{\nabla}_{\vec{k}}E(\vec{k})|} \qquad \text{(II.33)}$$

where dS is the surface element of a sheet of constant energy in wavevector space. The factor $\frac{(2\pi)^3}{\Omega_{cell}}$ is the volume between adjacent sheets of constant E in $\vec{k}$-space and Ω_{cell} is the unit cell volume in direct space. When $|\vec{\nabla}_{\vec{k}}E(\vec{k})| = 0$, where the energy bands are flat, the peaks occur in the density of states structure. So the band structure can be predicted by looking at the density of states structure. Points in $\vec{k}$-space where $|\vec{\nabla}_{\vec{k}}E(\vec{k})| = 0$ condition is fulfilled are

called critical points and the unusual structures they produce in the density of states (like jump discontinuities, infinite slope, discontinuous slope, logarithmic infinities, etc.) are called the van-Hove singularities. The kind of van-Hove singularities gives information about the dimensionality of the system.

II.5 Effective Mass

In a solid, the electron wavefunction is a Bloch wave and the energy depends upon the periodic potential $V(\vec{r})$ of the lattice. Near the minima, the energy of an electron in a solid is frequently quadratic in the components of the $\vec{k}$-vector. It is then possible to write

$$E \approx \frac{\hbar^2 k^2}{2m^*} + E_0 \tag{II.34}$$

where m^* is the effective mass of the electron.

To find an expression for the effective mass, one can start with the group velocity for an electron in terms of its energy band:

$$v_g = \frac{d\omega}{dk} = \frac{1}{\hbar}\frac{dE}{dk}. \tag{II.35}$$

If we take the time derivative of group velocity, the acceleration becomes

$$a = \frac{dv_g}{dt} = \frac{1}{\hbar}\frac{d}{dt}\left(\frac{dE}{dk}\right) = \frac{1}{\hbar}\left(\frac{d^2 E}{dk^2}\right)\frac{dk}{dt} = \frac{1}{\hbar^2}\left(\frac{d^2 E}{dk^2}\right)\frac{d(\hbar k)}{dt}. \tag{II.36}$$

Since the force can be written as

$$F = \frac{dp}{dt} = \hbar\frac{dk}{dt}. \tag{II.37}$$

Then comparing the two equations the acceleration will have the form

$$a = \frac{1}{\hbar^2}\left(\frac{d^2 E}{dk^2}\right)\frac{d(\hbar k)}{dt} = \frac{1}{\hbar^2}\left(\frac{d^2 E}{dk^2}\right)F. \tag{II.38}$$

¿From the Newton's second law of motion, $\vec{F} = m\vec{a}$, it can be recognized that

$$m^* = \frac{1}{\frac{1}{\hbar^2}\left(\frac{d^2 E}{dk^2}\right)}.$$
(II.39)

where it shows that the curvature of the energy band affects the inertia of the electron in that band. In the presence of anisotropy this will be reflected in the definition of the effective mass as well, which then has a tensorial form:

$$\left(\frac{1}{m^*}\right)_{\alpha\beta} = \frac{1}{\hbar^2}\left(\frac{\partial^2 E}{\partial k_\alpha \partial k_\beta}\right)$$
(II.40)

Effective mass is a measurable quantity, which can be obtained from cyclotron resonance experiment. Here we calculate the effective mass from the curvature of the energy band. The effective mass of a semiconductor can be obtained by fitting the actual $E(\vec{k})$ diagram around the conduction band minimum or the valence band maximum by a paraboloid. The $E(\vec{k})$ curve is concave at the bottom of the CB, so m^* is positive. Whereas, it is convex at the top of the valence band, thus m^* is negative. This means that a particle in that state will be accelerated by the field in the reverse direction expected for a negatively charged electron. That is, it behaves as if a positive charge and mass. This is the concept of the hole.

Thus, for more parabolic bands, the electron will be lighter and for less parabolic (more flat) it will have a heavier mass.

CHAPTER III

STRUCTURE OF TlSe

There are a series of compounds that can be called TlSe-type crystals which are TlGaTe$_2$, TlInTe$_2$, TlInSe$_2$, and TlSe. The other type is TlGaSe$_2$ structure which are TlGaS$_2$, TlS, TlInS$_2$, and TlGaSe$_2$. TlSe-type shows chain structure behavior while the other type shows layered structure behavior. Actually the formula of TlSe is more informative if written in terms of different charge states it possesses as Tl$^+$(Tl^{3+}Se$_2^{2-}$)$^-$, or in general, Tl$^+$(M^{3+}X$_2^{2-}$)$^-$ where M is Tl, Ga or In, and X is Se, S, or Te. In the crystal for the TlSe, trivalent thallium atoms (Tl^{3+}) make a chain along the z axis, which corresponds to the optical c axis, and binds to selenium covalently in a tetrahedral shape. Monovalent thallium atoms (Tl$^+$) also bind to divalent selenium atoms (Se^{2-}) but weakly in an octahedral environment. For TlInSe$_2$, In atoms take the place of trivalent Tl^{3+} atoms. Binding ionically with Tl atoms gives a natural cleavage along the (110) plane.

22

TlSe-type is a mixed-valence compound containing monovalent and trivalent Tl atoms. This property makes the TlSe a ternary compound. The single crystals of the ternary compounds, a typical one being $TlInSe_2$, are of great interest. Their electrical parameters are sensitive to temperature, to pressure, and to the influence of electromagnetic waves. Because of this sensitivity, they exhibit switching and memory capability. The switching from the semiconductor case to the metal case occurs under the influence of large electric field in the direction (110) [13]. The non-linear transport properties [14] lead to possible technological applications such as oscillators and thermistors. The ternary compounds $TlInX_2$ (X=Se, Te) in general show nonlinear electrical behavior at moderate and higher current densities while ohmic behavior at low current densities [15]. Its reason is supposed to be due to electrothermal property of the material in the ref [13]. At pressures higher than $\cong 0.7$ GPa $TlInSe_2$ is non-transparent to a laser light with energy 1.17 eV [16]. According to the study of hydrostatic pressure on the electrical conductivity of $TlInSe_2$, the band gap of $TlInSe_2$ crystal decreases with increasing pressure [17]. The metallic conductivity of TlSe shows interesting behavior at low temperatures. In the low temperature interval, between 4.2–1.3 K, TlSe gives two types of results. In one case the resistivity rises with decreasing temperature with a low activation energy at about 1 meV while in the other case the resistivity does not change at all [17]. The chain-like ternary compounds are also important for obtaining high quality heterojunctions. For this purpose, the liquid TlSe

is melted on the natural (110) cleavage surface of TlInSe$_2$ [18]. According to this study, it is important for the isotropic compounds to have natural surface with a low density of states for obtaining the good heterojunctions. They also pointed out that this structure is sensitive to light (near-IR) and exhibits high radiation resistance.

Panich and Gasanly [19] performed a nuclear magnetic resonance (NMR) measurements to study the indirect nuclear exchange coupling, electronic structure, and wave-functions overlap for the single crystal of semiconductor TlSe. They reported strong exchange coupling among the spins of Tl$^+$ and Tl^{3+} ions due to the overlap of the Tl$^+$ and Tl^{3+} electron wave functions across the intervening Se atoms. They found this interaction was significantly stronger than the exchange coupling of the nuclei of the equivalent atoms within the chains. According to their study, the wave-function overlap of monovalent and trivalent thallium atoms is the dominant mechanism of the formation of the uppermost valence bands and lower conduction bands in TlSe and determines the electronic structure and the main properties of the compound.

The chain-like compounds are in the III-VI compound family. The shape of the unit cell of TlSe is the body centered tetragonal (*bct*) which belongs to D_{4h}^{I8} ($I4/mcm$) space group. The atomic positions, primitive translation vectors and bond lengths between neighboring atoms are the parameters that describe the crystal structure and will be input in tight binding calculations. The atomic positions are given in Table III.1 and indicated in Fig. III.1.
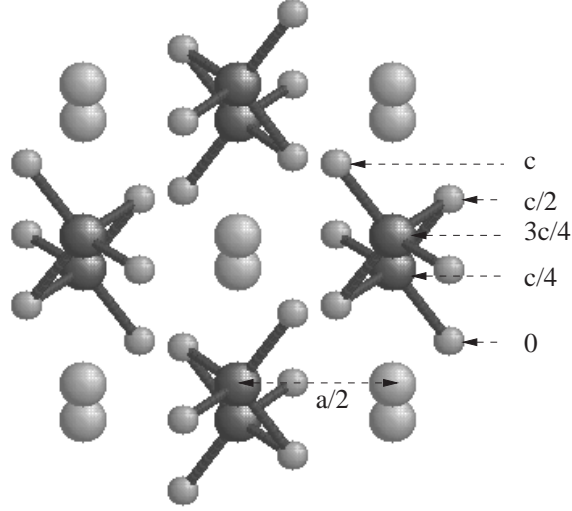
Figure III.1: Oblique view of the crystal structure for TlSe. The large light spheres are Tl^+ ions, large dark spheres are Tl^{3+} ions and small light spheres are the Se^{2-} ions.

In Table III.1, $\eta = 0.358$ is the internal parameter, $a = 8.02 \pm 0.01$ Å and $c = 7.00$ Å are the lattice parameters of TlSe [20, 21]. The corresponding values for TlInSe$_2$ are given as $\eta = 0.3428$, $a = 8.075$ Å, and $c = 6.847$ Å [22]. The atomic positions for each compound are listed in Table III.1. There are 8 atoms in each unit cell. The primitive translation vectors can be chosen as $(-a/2, a/2, c/2)$, $(a/2, -a/2, c/2)$, and $(a/2, a/2, -c/2)$.

Table III.1: The description of the unit cell.

# of ions	type of ions	positions of ions	TlSe (Å)	TlInSe$_2$ (Å)
2	$Tl(In)^{3+}$	$\pm(0, 0, c/4)$	(0, 0, 1.75)	(0, 0, 1.711)
2	Tl^+	$\pm(a/2, 0,$ c/4)	(4.01, 0, 1.75)	(4.03, 0, 1.71)
4	Se^{2-}	$\pm(\eta a/2, \eta a/2, \pm c/2)$	(1.43, 1.43, 3.5)	(1.38, 1.38, 3.42)

Table III.2: The first nearest neighbor atom distances

Bond	Length for TlSe (Å)	Length for TlInSe$_2$ (Å)
Tl^{3+}– Se^{2-}	2.68	2.60
Tl^{+} – Se^{2-}	3.428	3.448
Tl^{n+}– Tl^{n+}	3.50	3.424
Se^{2-}– Se^{2-}	3.853	3.866
Tl^{3+}– Tl^{+}	4.01	4.0375

The distances between any pair can be calculated using the atomic positions given in Table III.1 and the lattice parameters. The results for typical close neighbors are shown in Table III.2. These bond lengths compare reasonable with the sum obtained from the ionic bond of Se^{2-} and covalent bonds of Tl^{+} and Tl^{3+}.

The shape of the first Brillouin zone of the *bct* structure is given in the Figure III.2. The high symmetry points of this Brillouin zone are listed in Table III.3 and the symmetry lines are $K = (k, \pi/a, \pi/c)$ $D = (\pi/a, \pi/a, k)$, $\Sigma = (k, k, 0)$, $\Delta = (0, k, 0)$, $A = (0, 0, k)$, and $G = (k, 2\pi/a - k, 0)$.
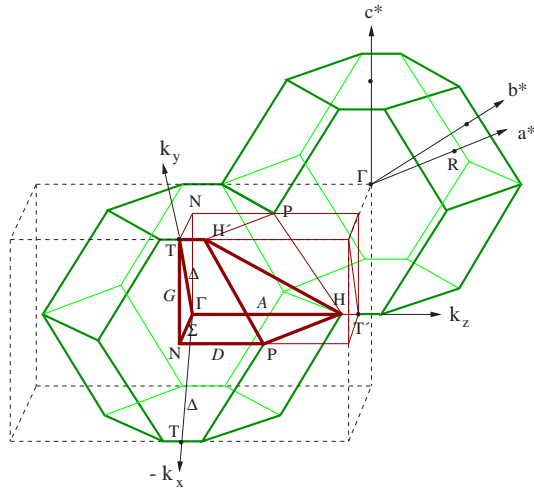

Figure III.2: The wedge shown in dark lines is the IR part (1/16) of the first Brillouin Zone.

Table III.3: The high symmetry points and these values in units of Å for TlSe and TlInSe$_2$. The parameter u is the ratio of c/a

	Symmetry Points	TlSe	TlInSe$_2$
R	$(0, \pi/a, \pi/c)$	$(0, 0.3917, 0.4487)$	$(0, 0.3890, 0.4588)$
P	$(\pi/a, \pi/a, \pi/c)$	$(0.3917, 0.3917, 0.4487)$	$(0.3890, 0.3890, 0.4588)$
N	$(\pi/a, \pi/a, 0)$	$(0.3917, 0.3917, 0)$	$(0.3890, 0.3890, 0)$
Γ	$(0, 0, 0)$	$(0, 0, 0)$	$(0, 0, 0)$
T	$(0, 2\pi/a, 0)$	$(0, 0.7834, 0)$	$(0, 0.7781, 0)$
T$'$	$(0, 0, 2\pi/c)$	$(0, 0, 0.897)$	$(0, 0, 0.9176)$
H	$(0, 0, (1+u^2)\pi/c)$	$(0, 0, 0.7905)$	$(0, 0, 0.7886)$

There are few theoretical studies to investigate the electronic structure of TlSe-type compounds. Gashimzade and Guliev [23] founded the band structure of TlSe-type for TlGaTe$_2$ by using an empirical pseudopotential model. The pseudo-potential method also used to find the energy band structure of TlSe in the Ref. [24]. The band structure of ternary chain TlInSe$_2$ is calculated by a pseudo-potential method with allowance for non-locality of ionic pseudo-potentials [25]. Another calculation has been done for TlGaTe$_2$ in the local-density approximation (LDA) using a full potential, with scalar-relativistic implementation of the linear augmented plane-wave (LAPW) method [14]. In a later study, the electronic structure of TlSe was investigated using an *ab initio* pseudopotential calculation in the density functional theory within the local density approximation (LDA) [26]. To our knowledge there is no published band structure for TlSe and TlInSe$_2$ obtained by tight binding method and no set of empirical parameters in the literature. The comparison of our results with the above calculations are presented in the next chapter.

CHAPTER IV

ELECTRONIC PROPERTIES

IV.1 TlSe

The energy band diagram of TlSe is obtained using the empirical tight-binding method whose interaction parameters (two-center integrals) are determined by fitting to ab initio LDA results [26]. The empirical tight binding method is used in its simplest form, which utilizes the orthogonal basis set and excludes three center interactions and in addition to on-site energies first and second nearest neighbor interactions are included. The atomic orbital configurations $Tl^+(6s^26p^1 \rightarrow 6s^26p^0)$, $Tl^{3+}(6s^26p^1 \rightarrow 6s^06p^0)$, and $Se^{2-}(4s^24p^4 \rightarrow 4s^24p^6)$ are treated as the valence electrons. In other words, sp^3 basis set is used for both kinds of atoms and in the expansion of the total wavefunction.

To find the energy eigenvalues we needed to fit totally 60 independent parameters for the sp^3 basis set. 6 parameters come from the on-site terms,

24 of them are the first nearest neighbor two-center integrals, and the other 24 parameters are the second nearest neighbor two-center integrals. 6 parameters are the extra *sp* interactions coming from the switching of the different atoms. There are some earlier methods proposed to fit these parameters [27] and used by other researchers [28]. Harrison [27] proposed for sc, bcc, fcc, and tetrahedral diamond structure that the hopping integrals can be found using the equation below :

$$V_{llm} = \eta_{llm} \frac{\hbar^2}{md^2} \tag{IV.1}$$

where d is the first nearest neighbor distance, and the m in the denominator is the electron mass. According to structure shape, η_{llm} has different values. Using these coefficients in the scaling law, the matrix elements can also be estimated for tetrahedral structure [29] as:

$$V_{\alpha\beta\gamma} = \eta_{\alpha\beta\gamma} \frac{e^{-2.5(\frac{R}{d}-1)}}{d^2} \tag{IV.2}$$

where d is the nearest neighbor distance between atoms of the same nature as those under consideration, and R is the actual distance between the atoms under consideration. These methods were not expected to give successful results when applied to III-VI compounds, GaSe and InSe [30]. So their fitting procedure was achieved by employing least-square fits to pseudopotential bands [31, 32, 33]. We applied Harrison's formula and scaling law to find the hopping integrals of TlSe and TlInSe$_2$, but as expected they did not give good results.

Instead, a careful study of the results for partial density of states obtained from the *ab initio* calculation of TlSe [26], revealed that 3 parameters were

enough to give the shape of semi core states (−14.0 to −12.0 eV), namely, the first and second nearest-neighbor interactions of s-orbitals ($(ss\sigma)_1$ and $(ss\sigma)_2$) for Se^{2-}-Se^{2-}, and the first nearest-neighbor interaction of s-orbitals of Tl^{3+}-Se^{2-} with the on-site term of Se^{2-} at 19.92 eV. Similarly, the four lower valence bands localized between −7.1 eV and −4.0 eV above the semi core states can be fitted by varying the parameters which are $(sp\sigma)$ interaction between Tl^{3+}-Se^{2-} and Tl^+-Se^{2-}, $(ss\sigma)$ and $(sp\sigma)$ interactions between any Tl ions. Although some other coefficients still affect slightly the shape of four bands, they are usually not significant. The same parameters also adjust the highest valence band and the lowest two conduction bands. But the lowest two conduction bands are actually affected also by the $(pp\sigma)$ and $(pp\pi)$ interaction parameters between Tl^{3+}-Tl^{3+} and Tl^+-Tl^+.

The 8 higher valence bands above the four lower valence bands are originated from $(pp\sigma)$ interaction between Se^{2-} ions and interaction between the p orbitals of Se^{2-} ions and p orbitals of monovalent and trivalent thallium ions.

Finally, interaction between the p orbitals of monovalent and trivalent thallium atoms made up the conduction bands.

The hopping integral parameters obtained by fitting to the results of ab-initio calculation [26] of TlSe are listed in the Table IV.1 and Table IV.2.

To obtain the energy band diagram of the TlSe, shown in Fig. IV.1, the lattice constants and the positions of the atoms in the Table III.1, the primitive translation vectors, the high symmetry points in the Brillouin zone, the bond

Table IV.1: The on-site energy parameters for TlSe

Ions	E_s(eV)	E_p(eV)
Tl^{3+}	−9.32	−3.51
Tl^{+}	−11.90	−2.01
Se^{2-}	−19.92	−9.55

Table IV.2: The first and second nearest neighbor two-center integral parameters (in eV) for TlSe

1st nearest-neighbors	$(ss\sigma)_1$	$(sp\sigma)_1$	$(ps\sigma)_1$	$(pp\sigma)_1$	$(pp\pi)_1$
Tl^{+}– Tl^{+}	−0.05	0.67	–	1.2	−0.60
Tl^{+}– Tl^{3+}	−0.05	−0.50	−0.40	0.3	−0.20
Tl^{+}– Se^{2-}	0.10	0.74	0.75	0.8	−0.30
Tl^{3+}– Tl^{3+}	0.28	−0.74	–	1.5	−0.20
Tl^{3+}– Se^{2-}	0.30	2.15	−1.00	1.2	−0.16
Se^{2-}– Se^{2-}	−0.10	0.10	–	0.5	−0.05
2nd nearest-neighbors	$(ss\sigma)_2$	$(sp\sigma)_2$	$(ps\sigma)_2$	$(pp\sigma)_2$	$(pp\pi)_2$
Tl^{+}– Tl^{+}	−0.01	0.0	–	−0.20	−0.10
Tl^{+}– Tl^{3+}	−0.08	0.08	0.0	0.10	−0.05
Tl^{+}– Se^{2-}	0.0	0.0	0.0	0.0	0.0
Tl^{3+}– Tl^{3+}	0.15	0.0	–	0.10	0.06
Tl^{3+}– Se^{2-}	0.0	−0.20	0.0	0.10	0.0
Se^{2-}– Se^{2-}	−0.09	0.0	–	−0.04	0.0

lengths of the crystal in Table III.3, and the fitting parameters in the Table IV.1 and IV.2 are used as input parameters for our tight binding code. Energy bands are given along symmetry lines of IR part of the first Brillouin zone (see Table III.2) which are sampled with 20 point meshes.

The maximum and minimum of the valence bands occur at the same symmetry point, T. So the width of the valence bands between these two points is fitted to the ab initio result of 7.41 eV [26].

The minimum of the conduction bands occur at a point between P and N along the line D.
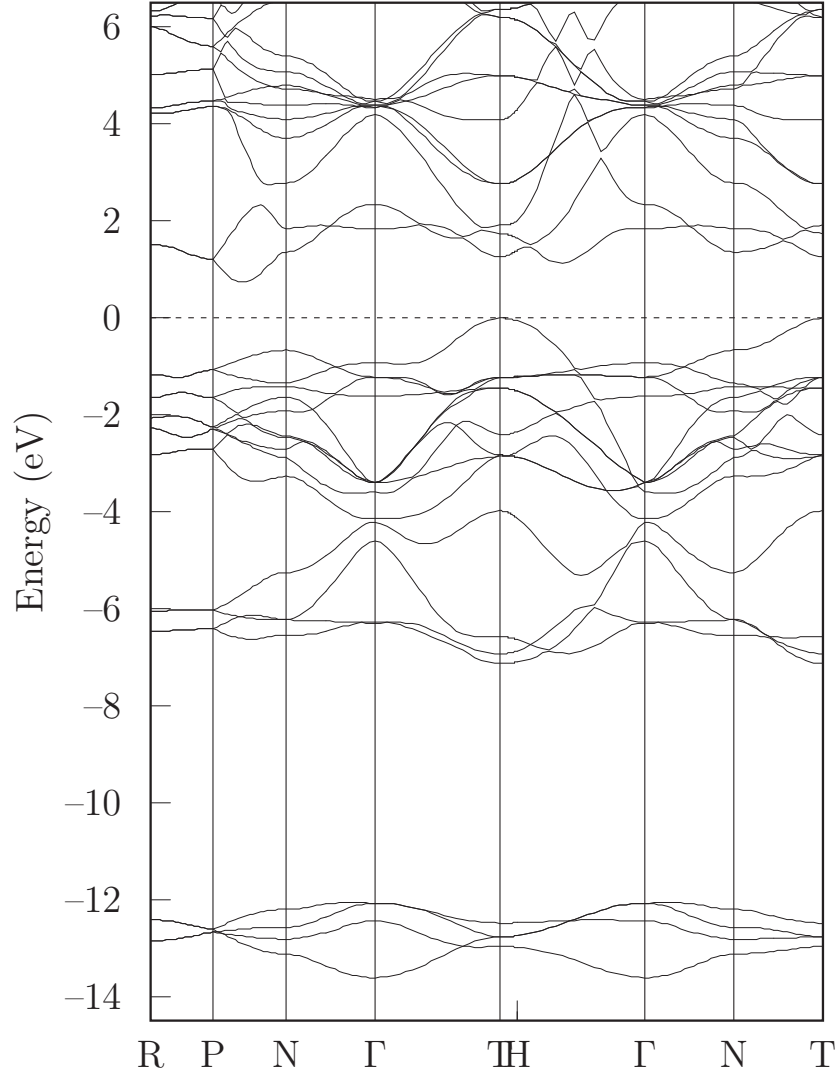
Figure IV.1: Tight binding results for the energy band structure of TlSe.

From the eigenfunction obtained for the same set of parameters we obtained the partial and total density of states.

From the partial density of states calculation in the Fig. IV.2, the lowest valence bands at the bottom are due to s-orbitals of Se^{2-} ions. The four valence bands above the first four bands result from mostly s-states of trivalent thallium ions and s-states of monovalent thallium ions. The Fig. IV.2 depicts that the upper valence band group correspond to mainly p-states of Se^{2-} ions.
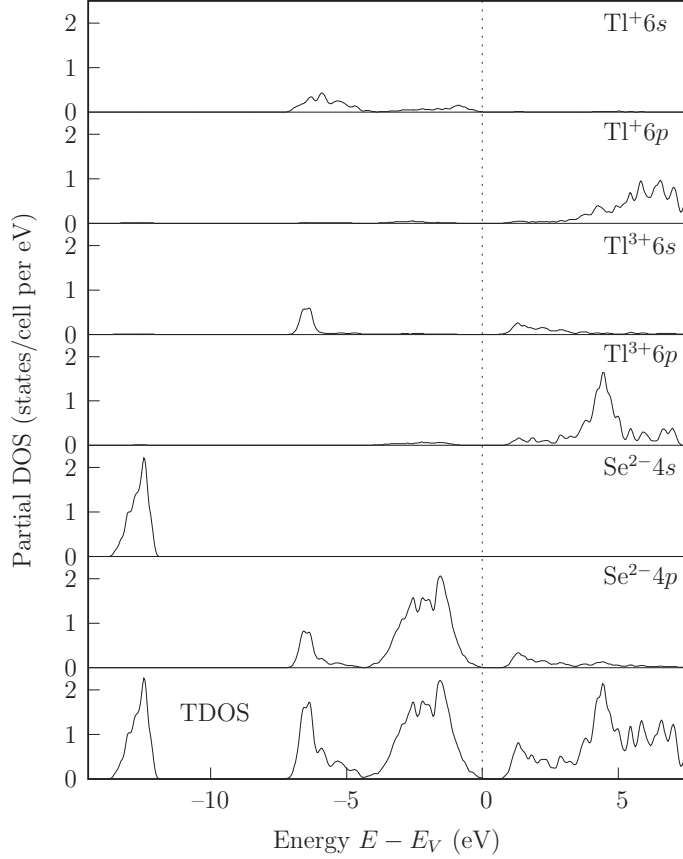
Figure IV.2: Partial densities of states for TlSe.

s and p orbitals of Tl^{3+} ions and p-orbitals of Se^{2-} form the lowest conduction bands. We cannot discuss charge density in the upper conduction bands because of the disagreement of the energy bands.

IV.2   Comparison of the results of TlSe

Starting from the lower energies upward, the comparison of the tight-binding results to the *ab initio* LDA results shown in Figs. IV.1 and IV.3, respectively, reveals the following observations: the shape of the semi-core bands and the way they disperse are the same.
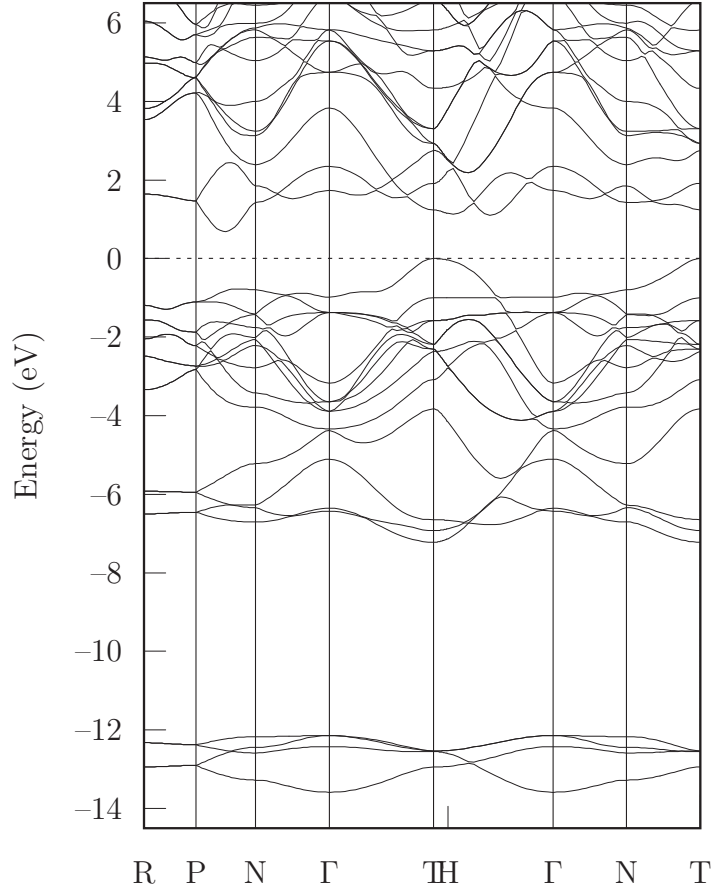
Figure IV.3: Ab initio results for the energy band structure of TlSe [26].

The four lower valence bands are in a good agreement with the *ab initio* calculation and separated from the upper valence bands as in the *ab initio* result. This agreement also valid for the rest of the valence bands. When we look at the study of band structure of ternary chain TlSe-type crystals [23], we can not see this agreement. According to their calculation, the lowest two bands separated from the upper valence bands, and the top valence bands are far from the rest of the valence band group, and their shape are different from our calculation. In our calculation, the edge of the valence bands, including the lowest and the highest valence bands, are exactly fitted on the *ab initio*

34

bands. The valence width is found same with the *ab initio* result which is 7.21 eV. The valence bands from top to bottom have almost the same shape, but some differences can still be seen in detail.

When we look at the conduction bands, we were hardly able to fit only the lowest three bands. For the two lowest conduction bands, there is a disagreement along the A line between the symmetry points H and Γ. Along this line these two lowest conduction bands must have been separated from the upper conduction bands. But great achievement has come from obtaining the first and the second minimum points of the lowest conduction band which are exactly at the same symmetry points with the result of *ab initio* calculation. According to result of *ab initio* method [26], the expected band gap is underestimated due to the artifact of Local Density Approximation. The fitting has been done to results where the conduction bands are shifted upwards by 0.8 eV. This shifting was necessary due to fit the band gap to the experimental results which is found between 0.6–1.0 eV by different authors [34, 35]. The band gap for TlSe is found as 0.73 eV in Ref. [24]. The agreement for the values of the first and the second minimum, respectively at 0.69 eV and 1.11 eV can be seen after the shifting process. The third minimum point of conduction band is appeared at the symmetry point T instead of H. But this still gives the direct gap at the same value which is 1.17 eV.

When we obtained the total density of states with using the tight binding method, we saw great agreement with the ab-initio results. The shape of the

TDOS for the valence bands is almost same, but we saw the differences in the conduction band states. The results in the Fig. IV.2 consistent with *ab initio* PDOS calculation [26]. In the study of TlSe with *ab initio* method, it is found that *s*-like character due to $6s^2$ of Tl^+ ions are participating in the valence bands at the high symmetry point T. They did not find contribution of Tl^+ ions in the anti-bonding bands, which were formed by Tl^{3+} $6s$ and Se^{2-} $4p$ states. When they plotted the charge density of (004) plane of TlSe, they noticed $6p$ and $6s$ electrons of trivalent thallium had some charge density extending towards Se^{2-} ions.
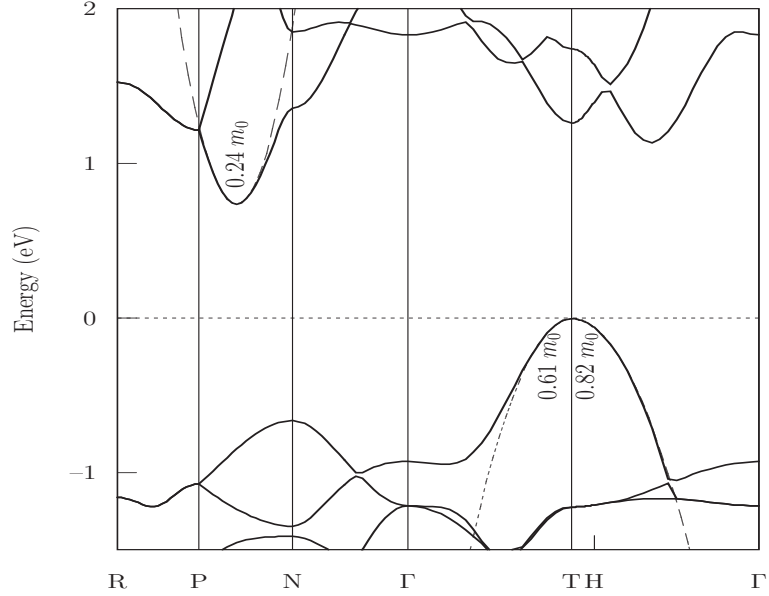

Figure IV.4: Parabola fitting to the conduction band minimum and valence band maximum for TlSe.

The effective masses are calculated by fitting the energy bands by parabolas. Fig. IV.4 below depicts the fitting procedure at the bottom of the conduction band by a parabola which gives the value of 0.24 m_0 where m_0 is the free electron mass equal to 9.10938×10^{-31} kg.

36

Table IV.3: The effective masses for TlSe along high symmetry directions.

High symmetry points and lines	ETB results	ab-initio results
Hole at T	$m_h^* = 0.65 \, m_0$	$m_h^* = 0.33 \, m_0$
Hole at H	$m_h^* = 0.81 \, m_0$	$m_h^* = 1.16 \, m_0$
e^- along D	$m_e^* = 0.24 \, m_0$	$m_e^* = 0.16 \, m_0$
e^- along A between H-Γ	$m_e^* = 0.427 \, m_0$	$m_e^* = 0.22 \, m_0$
e^- at H		$m_e^* = 0.34 \, m_0$
e^- at T	$m_e^* = 0.407 \, m_0$	$m_e^* = 0.37 \, m_0$
e^- at T along G	$m_e^* = 0.637 \, m_0$	$m_e^* = 0.38 \, m_0$

In the Table IV.3, the effective masses are represented for the result of the tight binding method and for the result of *ab initio*. The values can be hardly compared because of the differences of the curvatures of the bands, but the heaviest hole for both result appears at the same high symmetry point H and the smallest value for the electron appear again along the same high symmetry line D. Other theoretical result for effective masses of TlSe are presented by Gashimzade and Orudzhev [36] who calculated the band structure of TlSe using the pseudo-potential method and the effective masses were found by using the $\vec{k} \cdot \vec{p}$ method. According to their study, the effective masses of holes were $m_\perp^* = 0.32 \, m_0$ and $m_\parallel^* = 4.40 \, m_0$, where $m_\parallel^*$ is the effective mass of holes in the direction parallel to tetragonal axis. The electron masses were found to be $m_1^* = 0.840 \, m_0$, $m_2^* = 0.35 \, m_0$, and $m_3^* = 0.27 \, m_0$. The experimental results from the electrical conductivity, Hall effect, and thermoelectric power are $m_h^* = 0.6 \, m_0$, and $m_e^* = 0.3 \, m_0$ [37] and $m_h^* = 0.86 \, m_0$ [38].

IV.3 TlInSe$_2$

The band structure of another ternary chain, TlInSe$_2$, has also been investigated by the empirical tight binding approach, but this time the hopping integrals are fitted to the results of the pseudopotential method used by Orudzhev et al. [25] and their band structure is given in Fig. IV.5.
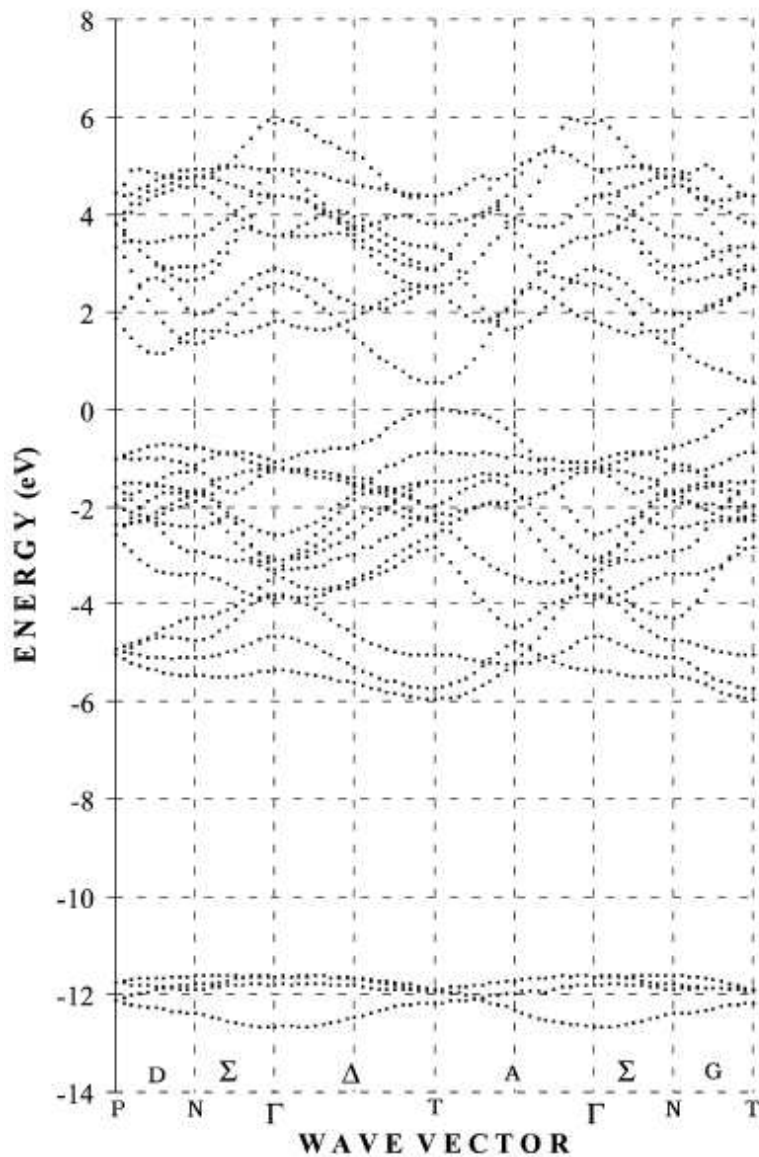

Figure IV.5: Pseudopotential Band Structure of TlInSe$_2$ [25].

The empirical tight-binding parameters obtained from this fit for TlInSe$_2$ are given in the tables below and the band structure is shown in Fig. IV.6.

Table IV.4: The on-site energies for TlInSe$_2$

Ions	E_s(eV)	E_p(eV)
In^{3+}	−7.52	−4.11
Tl^{+}	−10.80	−2.61
Se^{2-}	−19.22	−9.35

Table IV.5: The first and second nearest neighbor two-center integral parameters (in eV) for TlInSe$_2$

1st nearest-neighbors	$(ss\sigma)_1$	$(sp\sigma)_1$	$(ps\sigma)_1$	$(pp\sigma)_1$	$(pp\pi)_1$
Tl^{+}− Tl^{+}	−0.10	0.40	–	1.40	−0.60
Tl^{+}− In^{3+}	−0.10	−0.70	−0.05	0.30	−0.28
Tl^{+}− Se^{2-}	0.10	0.64	0.75	0.70	−0.30
In^{3+}− In^{3+}	0.15	−0.30	–	1.50	−0.50
In^{3+}− Se^{2-}	0.60	1.80	−1.00	1.40	−0.25
Se^{2-}− Se^{2-}	−0.04	0.10	–	0.45	−0.05
2nd nearest-neighbors	$(ss\sigma)_2$	$(sp\sigma)_2$	$(ps\sigma)_2$	$(pp\sigma)_2$	$(pp\pi)_2$
Tl^{+}− Tl^{+}	0.0	0.0	–	−0.20	−0.10
Tl^{+}− In^{3+}	0.0	0.1	0.0	0.10	−0.05
Tl^{+}− Se^{2-}	0.0	0.0	0.0	0.0	0.0
In^{3+}− In^{3+}	0.25	0.0	–	0.10	0.06
In^{3+}− Se^{2-}	0.0	−0.2	0.0	0.10	0.0
Se^{2-}− Se^{2-}	−0.10	0.0	–	−0.04	0.0

The agreement between the energy bands of TlInSe$_2$ obtained by our empirical tight binding method and the pseudopotential method [25] is remarkable, especially for the valence bands. The valence band edges, and the lowest conduction bands are fitted very well. The top of the valence band and the bottom of the conduction band are located at the symmetry point T as in the bands of the pseudopotential method. The direct band gap energy is obtained in agreement with their value of ≈ 0.6 eV.
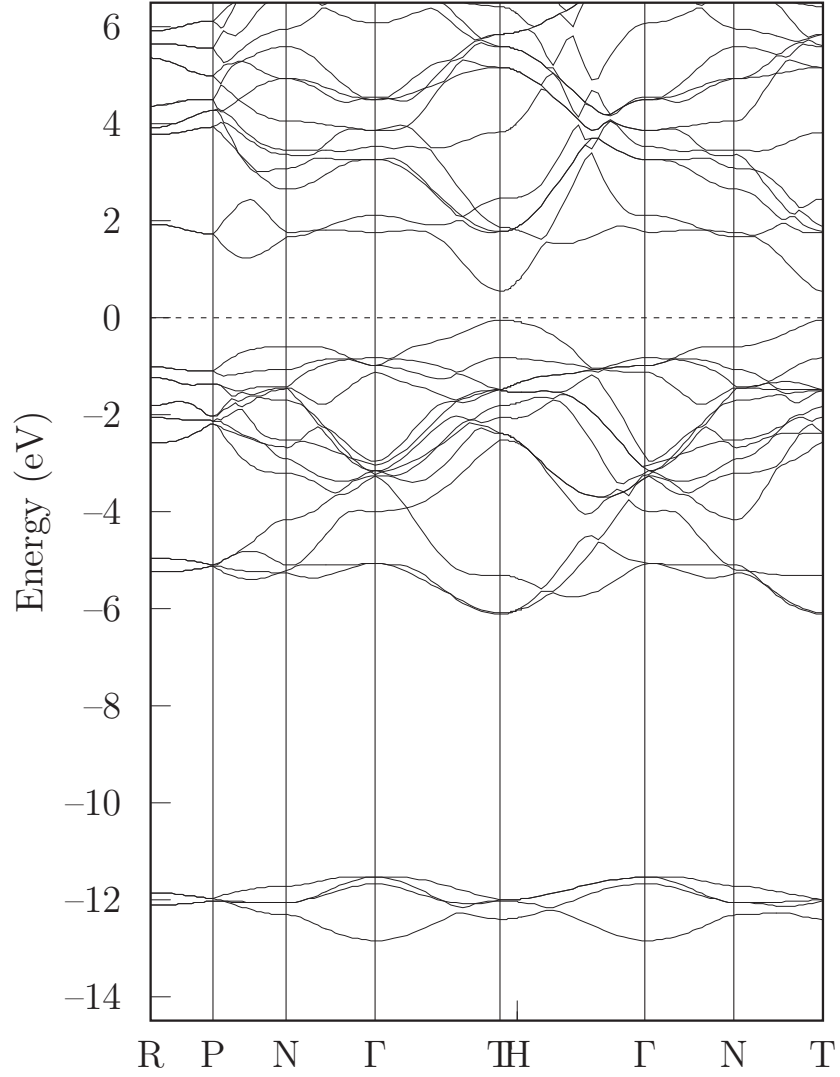
Figure IV.6: Tight Binding Band Structure of TlInSe$_2$.

In the experimental side, the optical band gap for TlInSe$_2$ is found to be indirect and reported as $\approx$ 1.4 eV at room temperature [39]. In another study the indirect band gap is claimed to be 1.2 eV [40]. The indirect and direct band gaps of TlInSe$_2$ are found 1.07 eV and 1.35 eV, respectively in a different study [41]. Since our energy bands and the parameters that produce them are obtained from the fit to the most recent calculations of the energy bands of TlInSe$_2$, our band gap is also fitted to their direct gap of 0.6 eV.
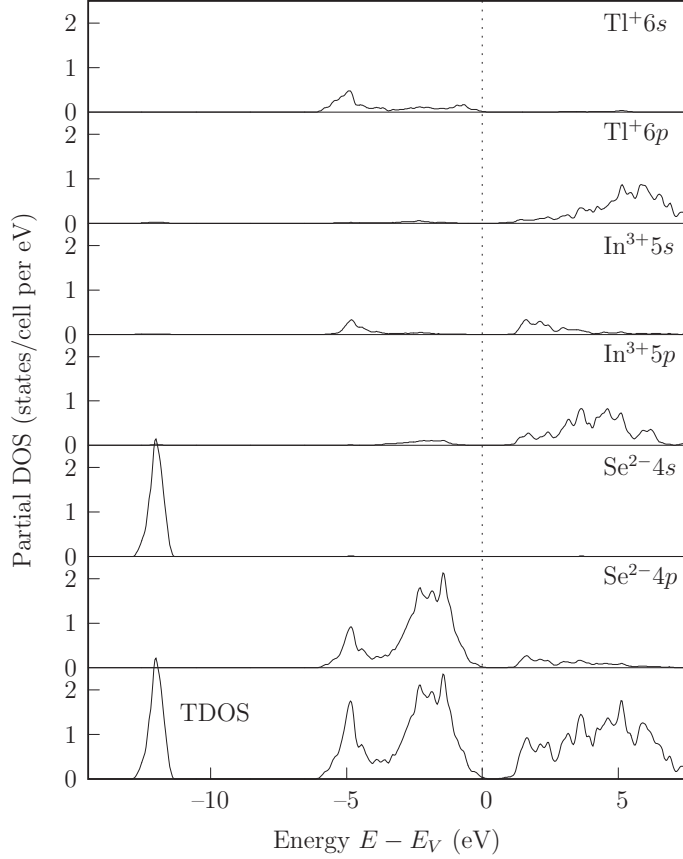
40

Figure IV.7: Partial densities of states for TlInSe$_2$.

PDOS and TDOS for TlInSe$_2$ are presented in the Fig. IV.7. We see very similar behavior in electron density of states when compared with the TlSe case. Since the structure of two compounds are the similar and the main difference being In^{3+} ions take the place of trivalent thallium ions, the shape of the density of the orbitals of In^{3+} is almost the same as Tl^{3+}. The peak occurring at about –12.0 eV due to s-states of Se^{2-} ions is narrower and sharper than the same peak for TlSe charge density. Other contributions of the orbitals from monovalent thallium and chalcogen ions are the same as in TlSe. In general, results agree well with the study of Orudzhev et al. [25].
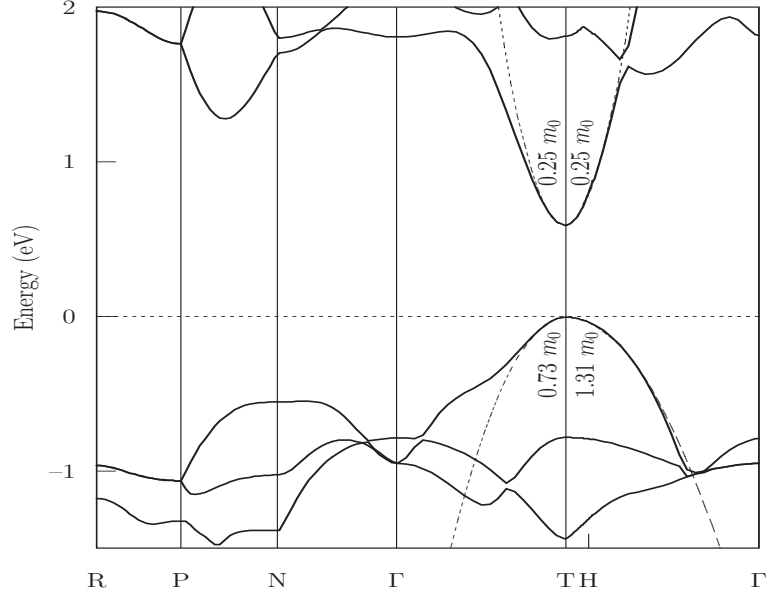
Figure IV.8: Effective mass estimation by parabola fitting to the bands of TlInSe$_2$.

The effective masses of holes and electrons for TlInSe$_2$ are found by fitting the bands by parabola. The effective masses of electrons are $m_e^* = 0.22\, m_0$ and $m_e^* = 0.29\, m_0$ respectively at the point T, and along the symmetry line D. The effective masses of holes are $m_h^* = 0.98\, m_0$ at T and $m_h^* = 1.2\, m_0$ at H. To our knowledge there are no data in the literature about the effective masses of TlInSe$_2$ to compare with our results.

CHAPTER V

CONCLUSION

The problem considered in this work is the electronical behavior of chain-like compounds, TlSe and TlInSe$_2$. For this purpose, simple tight binding model is used and tight binding parameters for these compounds are found by fitting the energy bands for TlSe to *ab initio* LDA results and for TlInSe$_2$ to pseudopotential method results. We have seen the simple tight binding method is enough to explain the behavior of the electron in the valence bands. This study showed us that tight binding method can be applied to chain-like compounds successfully.

We obtained the indirect band gap for TlSe, and direct band gap for TlInSe$_2$ and the second indirect transition for them in agreement with experimental and theoretical results but the third indirect transitions for TlSe were not in agreement with ab-initio results.

After partial density of states and total density of states calculations, the

contributions of the orbitals of the atoms were predicted well with the fitting parameters presented in the previous chapter. The results are found in good agreement with the previous theoretical and experimental results again in the valence band region.

The effective masses were calculated for TlSe and TlInSe$_2$ by fitting parabolas to the energy bands at extremum points. The curvatures of parabolas give effective masses of the electrons and holes.

REFERENCES

[1] Bloch F *Z. Phys.* **52** 555 (1928).

[2] J. C. Slater and G. F. Koster, *Phys. Rev.* B **94**, 1498 (1954).

[3] P. Löwdin, *J. Chem. Phys.* **18**, 365 (1950).

[4] K. C. Pandey, *Phys. Rev. B* **14**, 1557 (1976).

[5] L. F. Mattheiss and J. R. Patel, *Phys. Rev. B* **23**, 5384 (1981).

[6] D. A. Mirabella, C. M. Aldao, and R. R. Deza, *Phys. Rev.* B **50**, 12152 (1994).

[7] B. A. McKinnon and T. C. Choy, *Phys. Rev.* B **52**, 14531 (1995).

[8] P. Vogl, H. P. Hjalmarson, and J. D. Dow, *J. Phys. Chem. Solids* **44**, 365 (1983).

[9] Y. C. Chang and D. E. Aspnes, *Phys. Rev. B* **41**, 12002 (1990).

[10] J. M. Jancu, R. Scholz, F. Beltram, and F. Bassani, *Phys. Rev. B* **57**, 6493 (1998).

[11] D. A. Papaconstantopoulos, *Handbook of the Band Structures of Elemental Solids* (Plenum, New York, 1986).

[12] S. Kashida, T. Saito, M. Mori, Y. Tezuka, and S. Shin, *J Phys: Condens. Matter* **9**, 10271 (1997).

[13] A. G. Abdullaev and V K Aliev, *Mat. Res. Bull.* **15**, 1361 (1980).

[14] K. Okazaki, K. Tanaka, J. Matsuno, A. Fujimori, L. F. Mattheiss, S. Iida, E. Kerimova, and N. Mamedov, *Phys. Rev. B* **64**, 045210 (2001).

[15] M. Hanias, A. N. Anagnostopoulos, K. Kambas, and J. Spyridelis, *Phys. Rev. B* **43**, 4135 (1991).

[16] K. R. Allakhverdiev, N. Yu. Safarov, M. A. Nizametdinova, E. A. Vinogradov, N. N. Melnik, A. F. Goncharov, and S. I. Subbotin, *Solid State Commun.* **41**, 485 (1982)

[17] N. A. Abdullaev, M. A. Nizametdinova, A. D. Sardarly, and R. A. Suleymanov, *J Phys: Condens. Matter* **4**, 10361 (1992).

[18] I. V. Alekseev, *Semiconductors*, **32**, 526 (1998).

[19] A. M. Panich and N. M. Gasanly, *Phys. Rev. B* **63**, 195201 (2001).

[20] J. A. Ketelaar, W. H. t'Hart, M. Moerel, and D. Polder, Z. Kristallogr. **A101**, 396 (1939).

[21] R. W. G. Wyckoff, "Crystal Structures", 2nd edition, Vol. **2**, (Interscience, New York, N. Y., 1964).

[22] D. Muller, G. Eulenberger, H. Hahn, Uber ternare thalliumchalkogenide mit thalliumselenide structures, Z. Anorg. Allg. Chem. 398, 207-220 (1973)

[23] F. M. Gashimzade and D. G. Guliev, *phys. stat. sol. B* **131**, 201 (1985).

[24] G. I. Abutalybov, A. A. Aliev, M. A. Nizametdinova, G. S. Orudzhev, and R. Kh. Nani, *Fiz. Tekh. Poluprovodn.* **15**, 851 (1981) [*Sov. Phys. Semicond.* **15**, 486 (1980)].

[25] G. Orudzhev, N. Mamedov, H. Uchiki, N. Yamamoto, S. Iidia, H. Toyota, E. Gojaev, and F. Hashimzade, *J. Phys. Chem. Sol.* **64**, 1703 (2003).

[26] Ş Ellialtıoğlu, E. Mete, R. Shaltaf, K. Allakhverdiev, F. Gashimzade, M. Nizametdinova, and G Orudzhev, *Phys. Rev. B* **70**, 195118 (2004).

[27] W. A. Harrison, *Phys. Rev. B* **24**, 5835 (1981).

[28] F. M. Gashimzade (private communications).

[29] J. O. Fourcade, A. Ibanez, J. C. Jumas, M. Maurin, I. Lefebre, P. Lippens, M. Lannoo, and G. Allan, *J. Solid State Chem.* **87**, 366 (1990).

[30] M. O. D. Camara and A. Mauger, *Phys. Rev. B* **65**, 125206 (2002)

[31] G. Dresselhaus and A. M. Dresselhaus, *Phys. Rev.* **160**, 6491 (1967);

[32] K. C. Pandey and J. C. Phillips, *Phys. Rev. B* **13**, 750 (1976).

[33] J. N. Schulman and T. C. McGill, *ibid.* **19**, 6341 (1979).

[34] E. Mooser and W. B. Perason, *Phys. Rev.* **101**, 492 (1956).

[35] R. S. Itoga and C. R. Kannewurf, *J. Phys. Chem. Solids* **32**, 1099 (1971).

[36] F. M. Gashimzade and G. S. Orudzhev, *Fiz. Tekh. Poluprovodn.* **15**, 1311 (1981).

[37] G. D. Guseinov, G. A. Akhundov, and G. B. Abdullaev, *Fiz. Tverd. Tela* (Leningrad) **4**, 1206 (1962) [*Sov. Phys. Solid State* **4**, 885 (1962)].

[38] S. A. Aliev, M. A. Nizametdinova, Sh. O. Orudzheva, and S. I. Tairov, *Fiz. Tekh. Ploprovodn.* **5**, 567 (1971) [*Sov. Phys. Semicond.* **5**, 499 (1971)].

[39] E. Kerimova, S. Mustafaeva, D. Guseinova, I. Efendieva, S. Babaev, T.G. Mamedov, Z. Salaeva, and K. Allakhverdiev, *Phys. Stat. Sol. A* **179**, 199 (2000).

[40] A. E. Bakhyshov, M. F. Agaeva, and A. M. Darvish, *phys. stat. sol. (b)* **91**, K31 (1979).

[41] M. Hanias, A. Anagnostopoulos, K. Kambas, and J. Spyridelis, *Physica* (Utrecht) **160B**, 154 (1989).